energies

MDPI

Article

Simulation Study on Solar Single/Double-Effect Switching LiBr-H_2O Absorption Refrigeration System

Qingyang Li, Shiqi Zhao, Dechang Wang *, Qinglu Song *, Sai Zhou, Xiaohe Wang and Yanhui Li

College of Mechanical and Electrical Engineering, Qingdao University, Qingdao 266071, China
* Correspondence: dcwang@qdu.edu.cn (D.W.); sql@qdu.edu.cn (Q.S.); Tel.: +86-532-8595-0512 (D.W.)

Abstract: In this study, a solar single/double-effect switching LiBr-H_2O absorption refrigeration system was investigated to make full use of solar energy and give full play to the advantages of solar refrigeration systems. A corresponding thermodynamic dynamic mathematical model was developed. The operation characteristics of the system operating continuously for one week were analyzed. In order to highlight the advantages of the solar single/double-effect switching absorption refrigeration system, it was compared with other forms of solar refrigeration systems and compression refrigeration systems. The practical application potential of the single/double-effect switching LiBr-H_2O absorption refrigeration system was evaluated from the perspective of economy and environmental effect. The results showed that the system could achieve the switching operation between single-effect mode and double-effect mode under weather conditions of high solar radiation intensity, and the daily cooling efficiency on such days was relatively high. After an auxiliary heater was added, the primary energy savings of the solar single/double-effect switching LiBr-H_2O absorption refrigeration system were 25–52%, depending on the area of the collector and the volume of the storage tank. The solar fraction of the system was about 71.99% for continuous operation during the whole refrigeration season. However, the initial investment cost of the system equipment accounted for 89.66% of the total cost. Compared with the traditional compression refrigeration system, the initial investment cost of the solar single/double-effect switching LiBr-H_2O absorption refrigeration system was higher, but it had a better environmental protection effect.

Keywords: solar energy; single/double-effect absorption refrigeration; operation characteristics; economy; environmental analysis

Citation: Li, Q.; Zhao, S.; Wang, D.; Song, Q.; Zhou, S.; Wang, X.; Li, Y. Simulation Study on Solar Single/Double-Effect Switching LiBr-H_2O Absorption Refrigeration System. *Energies* **2023**, *16*, 3220. https://doi.org/10.3390/en16073220

Academic Editor: Carlo Renno

Received: 15 February 2023
Revised: 30 March 2023
Accepted: 31 March 2023
Published: 3 April 2023

1. Introduction

Energy and climate issues have always been the focus of the international community. With the continuous development of the global economy, the demand for refrigeration is increasing all over the world, and the number of air conditioners is also increasing. As a result, carbon emissions have increased [1]. More and more countries in the world have put forward the goal of net-zero emissions and the creation of clean, low-carbon, safe and efficient energy systems to realize the green and low-carbon transformation of economic development [2,3]. At the same time, renewable energy such as solar energy has attracted much attention. The solar refrigeration system has become a research hotspot because of its advantages of low carbon and environmental protection [4–6].

Up to the present, for research into solar absorption refrigeration systems (ARSs), simulation software has been used by scholars [7–9] or the performance or thermodynamic characteristics of the system have been experimentally studied [10–12]. It has been possible to obtain an efficient, economical and reliable refrigeration cycle mode and system-operation control scheme by researching and analyzing these refrigeration systems. It has also been possible to improve the economy of solar ARSs. In this way, the unsustainable impact on energy and the environment caused by the rising global refrigeration demand has been alleviated [13–15].

A number of scholars have numerically studied solar ARSs using different configurations [8,16]. Cheng et al. [17] developed a solar collector model and a single-effect absorption chiller model using TRNSYS and EES software, respectively. The operation characteristics of the single-effect LiBr-H_2O absorption chiller driven by solar energy were analyzed. The results showed that the low-temperature collector matched well with the single-effect LiBr-H_2O chiller. Shirazi et al. [18] put forward three different configurations of solar LiBr-H_2O absorption chillers according to the circulation mode of absorption chillers. The results showed that in a high solar radiation climate, in order to make a solar multi-effect refrigeration system more cost-effective than a single-effect refrigeration system driven by a vacuum tube collector, the cost of a parabolic trough collector needed to be reduced by about 20%. Muhammad et al. [19] compared and analyzed the operational characteristics of a solar double-effect LiBr-H_2O ARS using different cooling/heating auxiliary schemes. The comparison results showed that the primary energy saving rate of the system using the compressor refrigeration as the auxiliary device was significantly higher than that of the system using the auxiliary heater as the auxiliary device. However, the author mainly compared the energy-saving effects of different configuration schemes and did not comprehensively evaluate the system on the basis of economic and environmental benefits. Hang et al. [20] experimentally investigated the operational characteristics of a double-effect ARS driven by a parabolic trough collector. The economics of using natural gas as an auxiliary energy and a conventional compressor chiller as an auxiliary device were compared. It was shown that a solar refrigeration system with a conventional compressor chiller as auxiliary energy had better economic performance and environmental effects in terms of the whole life cycle of the system.

In order to further improve the economic and environmental benefits of solar refrigeration systems, Rahman et al. [21] conducted an experimental study on a new solar LiBr-H_2O absorption refrigeration air conditioner operating in the UAE climate. In addition to the vacuum tube collector, a solar photovoltaic panel was used to generate electricity to drive the pump and fan ensuring that the cooling system used 100% solar power as the driving force. The system had an additional energy-storage tank to ensure continuous operation of the refrigeration system. The cooling performance coefficient of the system was about 0.51. The system had a good application prospect in the UAE climate. In order to investigate the scalability and practicality of solar double-effect LiBr-H_2O ARSs in specific regions, Narayanan et al. [22] analyzed the feasibility of solar ARSs for application in subtropical climates in Australia. The results showed that solar refrigeration systems in subtropical climates could achieve solar fractions of up to 91%, and they could save AUD 1477 dollars per year in operating costs compared with compression refrigeration systems. However, the payback period of this system was too long—about 15.8 years. Therefore, the economic analysis of solar refrigeration systems is particularly important, and the payback period of the system needs to be reduced as much as possible [23].

With the deepening of the research into absorption refrigeration systems, in addition to the common single-effect, double-effect and multi-effect LiBr-H_2O ARSs, a new circulation mode has been proposed by Xu et al. [24]. The 0.n-effect and 1.n-effect variable-effect refrigeration cycles were suitable for the instability of low-temperature and medium-temperature solar heat sources. Theoretical analysis and experimental research was performed on the cycles. The concentration of the solution entering the low-pressure generator was changed by controlling the proportion of vapor generated by the high-pressure generator into the high-pressure absorber. The 1.n-effect refrigeration cycle was realized, so that the working temperature range of the cycle was increased (85–150 °C). In order to improve the performance of the variable-effect system, Zhang et al. [25,26] took coefficient of performance (*COP*) as the optimization objective to optimize *COP*, which was increased by 10.65%. Lubis et al. [27,28] experimentally studied the solar single/double-effect absorption chiller used in tropical Asia. Solar energy and gas were the driving heat source, and the system could operate in single- or double-effect mode. The overall performance of the system could be improved by adjusting the mass flow rate and the distribution ratio of the con-

centrated solution at the outlet of the absorber. Ma et al. [29] also analyzed the operation characteristics and economy of a new solar single/double-effect ARS.

The solar single/double-effect or variable-effect ARSs mentioned above were able to switch between different modes, but some of the internal components of such systems were used in both single-effect and double-effect modes, so the stability of these systems' operation needed to be further verified. Therefore, in this study, a new solar single/double-effect switching LiBr-H_2O chiller was proposed to improve the utilization range of the heat source temperature. The system is equipped with a single-effect chiller and a double-effect chiller. The current research on single- and double-effect chillers is very mature, so the system can be operated stably by combining single- and double-effect chillers. The practical application potential of the system was studied, and the economic and environmental effects of the system operating for the whole refrigeration season were analyzed. Based on the working principle of the solar ARS, a model of the solar single/double-effect switching LiBr-H_2O ARS was developed. The operating characteristics of the system operating continuously for a week in the cool season were simulated. The solar fraction, primary energy saving rate, leveling cost and CO_2 emissions of the system under different configuration conditions were compared and analyzed. In summary, the innovations of this work included the following points:

(1) A solar single/double-effect switching LiBr-H_2O ARS was proposed by combining single-effect and double-effect chillers.

(2) In order to analyze the feasibility of practical application of solar single/double-effect switching LiBr-H_2O ARSs, the economic and environmental effects of the system were analyzed.

2. System Description

The flowchart of the solar single/double-effect switching LiBr-H_2O ARS is shown in Figure 1. The main components of the system include the following: solar collector, storage tank, single-effect LiBr-H_2O absorption chiller (SACH), double-effect LiBr-H_2O absorption chiller (DACH), water pump and throttle valve. The hot water is heated by solar energy and stored in the storage tank. When the solar irradiation intensity is low but sufficient to heat the hot water to the start-up temperature of the SACH, electric valve EV2 opens and EV3 closes, and then the system starts to operate. The hot water flows to the single-effect generator, and the system operates in single-effect mode (SEM). When the solar irradiation intensity is high and the hot water temperature in the storage tank reaches the start-up temperature of the DACH, electric valve EV3 opens and EV2 closes. The hot water flows to the high-pressure generator, and the system switches from SEM to double-effect mode (DEM). When the intensity of solar irradiance is not enough to heat the hot water to the start-up temperature of the chiller, the auxiliary heat source can be used to heat the hot water to the temperature required under the rated working condition of the DEM. The auxiliary heat source maintains the stable operation of the system under the rated working condition of the DEM. When the auxiliary heat source is opened, electric valves EV3 and EV4 are opened at the same time. Electric valves EV2 and EV5 should be closed to ensure that the hot water only circulates between the auxiliary heater and the DACH, to prevent the hot water from returning to the water tank when the auxiliary heat source is powered. As a result, the heat dissipation of the storage tank and energy waste are avoided. For this study, in order to ensure stable operation of the system and make full use of solar energy, the start-up temperature of the chiller in SEM was set to 80 °C, and the switching temperature between SEM and DEM was set to 130 °C. The auxiliary heat source was, therefore, turned on when the outlet temperature of the tank was below 80 °C.

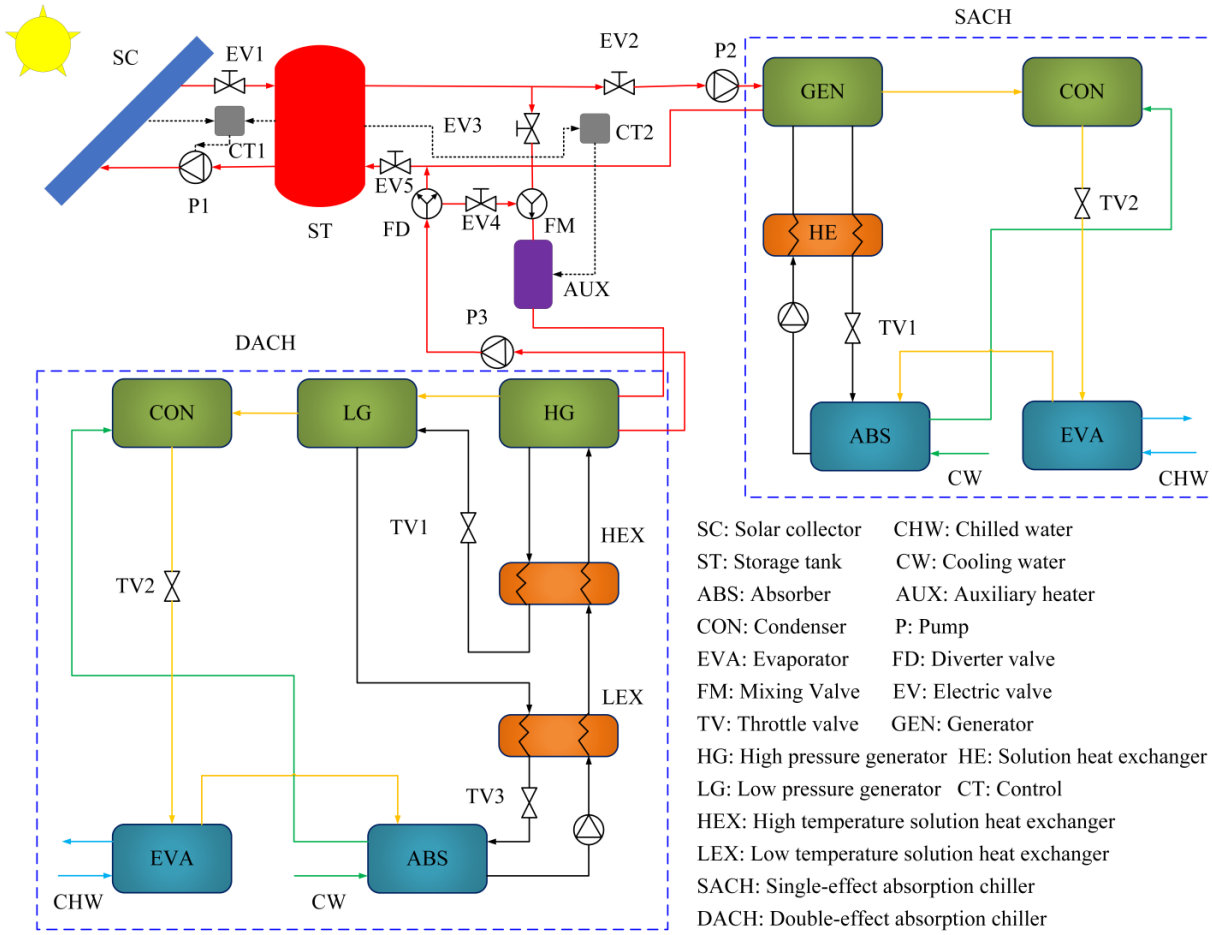

Figure 1. Schematic diagram of solar single/double-effect ARS.

3. Models and Methods

Models of the solar heat collection system and the LiBr-H_2O absorption chiller were developed in TRNSYS and EES, respectively, and then coupled in order to complete the simulation of the whole solar single/double-effect switching LiBr-H_2O ARS.

3.1. Model of Solar Heat Collection System

A model of the solar heat collection system was developed. The main components used in the simulation included the collector, storage tank, auxiliary heater, circulating water pump, and controller. For this study, we chose a vacuum tube collector to collect solar energy. The price of a vacuum tube heat collector is relatively cheap, and its heat collection temperature can reach the start-up temperature of the double-effect LiBr-H_2O absorption chiller. The mathematical model of the collector is as follows [30]:

$$Q_U = Q_S - Q_L = mc_p(T_i - T_a) \quad (1)$$

$$Q_S = AI_\theta(\tau\alpha)_e \quad (2)$$

$$\eta = \frac{Q_U}{AI_\theta} \quad (3)$$

where Q_U, Q_S and Q_L are the effective heat output by the collector per unit time, the solar heat absorbed by the collector, and the heat loss of the collector, respectively, W; A is the area of the heat absorbing plate, m^2; I_θ is the total radiation intensity absorbed by the collector, $W{\cdot}m^{-2}$; $(\tau\alpha)_e$ is the product of transmittance and absorbance; m and c_p are the instantaneous efficiency and efficiency factor of the collector, respectively, $kg{\cdot}s^{-1}$ and

J·kg^{-1}·°C^{-1}; U_L is the total heat loss coefficient of the collector, W·m^{-2}·°C^{-1}; T_i and T_a are the inlet temperature of the collector and the ambient temperature, respectively, °C.

The simplified mathematical model of the storage tank is as follows [30]:

$$C_t \frac{dT_s}{dt} = Q_U - Q_w - Q_{st} \tag{4}$$

$$Q_{st} = U_s A_s (T_{si} - T_a) \tag{5}$$

where C_t is the specific heat of the storage tank, J·kg^{-1}·°C^{-1}; Q_w and Q_{st} are the effective heat and heat dissipation of the storage tank, W; U_s is the heat transfer coefficient of water in the storage tank for heat exchange with the environment, W·m^{-2}·°C^{-1}; A_s is the internal surface area of the storage tank, m^2; T_{si} is the temperature of the hot water in the storage tank, °C.

3.2. Model of Absorption Refrigeration System

In order to reduce the complexity of the model and simulate the operating characteristics of the system, the following assumptions were made [31,32]:

- The internal pressure drop of each component of the system is negligible;
- Throttling devices are adiabatic;
- The low pressure generator and the condenser have the same pressure, the absorber and evaporator have the same pressure;
- The power of the solution pump is negligible.

Based on the working principle of a solar refrigeration system, the solar single/double-effect LiBr-H_2O ARS model was developed. The mathematical model of the double-effect chiller is as follows. The single-effect chiller model was developed in the same way. The mathematical models of each component were composed of mass conservation equation, energy conservation equation, heat transfer equation, with the thermophysical properties of the working fluid being directly taken from the library file of the EES v10 software. The mass conservation equation of lithium bromide should also be listed, using the concentration of lithium bromide solution for the generator, absorber and other components [33]. Then, the models of all components were connected in turn to develop the whole refrigeration cycle system [1,34].

High pressure generator

$$Q_{HG} = m_{hw} c_{hw} (T_{hwi} - T_{hwo}) \tag{6}$$

$$Q_{HG} = m_{hgo} h_{hgo} + m_{hgv} h_{hgv} - m_{hgi} h_{hgi} \tag{7}$$

$$Q_{HG} = (KA)_{hg} \Delta T_{hg} \tag{8}$$

$$m_{hgi} = m_{hgo} + m_{hgv} \tag{9}$$

$$m_{hgi} x_{hgi} = m_{hgo} x_{hgo} \tag{10}$$

Low pressure generator

$$Q_{LG} = m_{hgv} q_r \tag{11}$$

$$Q_{LG} = m_{lgv} h_{lgv} + m_{lgo} h_{lgo} - m_{lgi} h_{lgi} \tag{12}$$

$$m_{lgi} x_{lgi} = m_{lgo} x_{lgo} \tag{13}$$

$$m_{lgi} = m_{lgo} + m_{lgv} \tag{14}$$

Evaporator

$$m_{con} = m_{eva} \tag{15}$$

$$Q_{EVA} = c_{chw} m_{chw} (T_{chwi} - T_{chwo}) \tag{16}$$

$$Q_{\mathrm{EVA}} = m_{\mathrm{eva}} h_{\mathrm{eav}} - m_{\mathrm{con}} h_{\mathrm{con}} \tag{17}$$

$$Q_{\mathrm{EVA}} = (KA)_{\mathrm{eva}} \Delta T_{\mathrm{eva}} \tag{18}$$

Condenser

$$m_{\mathrm{vi}} = m_{\mathrm{lgv}} \tag{19}$$

$$m_{\mathrm{wi}} = m_{\mathrm{hgv}} \tag{20}$$

$$m_{\mathrm{vi}} + m_{\mathrm{wi}} = m_{\mathrm{con}} \tag{21}$$

$$Q_{\mathrm{CON}} = m_{\mathrm{vi}} h_{\mathrm{vi}} + m_{\mathrm{wi}} h_{\mathrm{wi}} - m_{\mathrm{con}} h_{\mathrm{con}} \tag{22}$$

$$Q_{\mathrm{CON}} = c_{\mathrm{cw}} m_{\mathrm{cw}} (T_{\mathrm{cwo}} - T_{\mathrm{cwi}}) \tag{23}$$

$$Q_{\mathrm{CON}} = (KA)_{\mathrm{con}} \Delta T_{\mathrm{con}} \tag{24}$$

Absorber

$$m_{\mathrm{abi}} = m_{\mathrm{lgo}} \tag{25}$$

$$m_{\mathrm{eva}} = m_{\mathrm{abv}} \tag{26}$$

$$x_{\mathrm{abi}} = x_{\mathrm{lgo}} \tag{27}$$

$$Q_{\mathrm{AB}} = m_{\mathrm{abi}} h_{\mathrm{abi}} + m_{\mathrm{abv}} h_{\mathrm{abv}} - m_{\mathrm{abo}} h_{\mathrm{abo}} \tag{28}$$

$$Q_{\mathrm{AB}} = m_{\mathrm{cw}} c_{\mathrm{aw}} (T_{\mathrm{awo}} - T_{\mathrm{awi}}) \tag{29}$$

$$Q_{\mathrm{AB}} = (KA)_{\mathrm{ab}} \Delta T_{\mathrm{ab}} \tag{30}$$

High temperature solution exchanger

$$Q_{\mathrm{HEX}} = m_{\mathrm{abo}} (h_{\mathrm{hgi}} - h_{\mathrm{hexi}}) \tag{31}$$

$$Q_{\mathrm{HEX}} = m_{\mathrm{hgo}} (h_{\mathrm{hgo}} - h_{\mathrm{lgi}}) \tag{32}$$

$$(h_{\mathrm{hgo}} - h_{\mathrm{lgi}}) = n (h_{\mathrm{hgo}} - h_{\mathrm{hexi}}) \tag{33}$$

Low temperature solution exchanger

$$Q_{\mathrm{LEX}} = m_{\mathrm{abo}} (h_{\mathrm{hexi}} - h_{\mathrm{abo}}) \tag{34}$$

$$Q_{\mathrm{LEX}} = m_{\mathrm{lgo}} (h_{\mathrm{lgo}} - h_{\mathrm{abi}}) \tag{35}$$

$$(h_{\mathrm{lgo}} - h_{\mathrm{abi}}) = n (h_{\mathrm{lgo}} - h_{\mathrm{abo}}) \tag{36}$$

The rated cooling capacity of the SEM and DEM of the system were 5 kW and 10 kW, respectively. Under the initial conditions, the area of the collector was 65 m^2 and the volume of the storage tank was 1 m^3.

3.3. Performance Evaluation

(1) Solar Fraction [35]

$$SF = \frac{\sum Q_{solar}}{\sum Q_{solar} + \sum Q_{aux}} \tag{37}$$

where SF is the fraction of solar energy utilized over a period of time, %; $\sum Q_{solar}$ is the accumulated heat from solar energy, kWh; $\sum Q_{aux}$ is the accumulated heat from auxiliary heat sources, respectively, kWh.

(2) Daily Cumulative Cooling Efficiency [30]

$$\eta_{\mathrm{d}} = \frac{\sum Q_{\mathrm{e,d}}}{\sum Q_{\mathrm{collector,d}}} \tag{38}$$

where η_{d} is the daily cooling efficiency of the system, %; $\sum Q_{\mathrm{e,d}}$ is the cumulative cooling capacity of the system in one day, kWh; $\sum Q_{\mathrm{collector,d}}$ is the accumulated heat collection capacity of the collector in one day, kWh.

(3) Primary Energy Saving Rate [19]

$$f_{\mathrm{sav}} = 1 - \frac{\sum Q_{\mathrm{aux}}}{\frac{\sum Q_{\mathrm{ref,e}}}{COP_{\mathrm{ref}}}} \tag{39}$$

where f_{sav} is the primary energy saving rate; $\sum Q_{\mathrm{aux}}$ is the accumulated heat consumption of the auxiliary heat source, kWh; $\sum Q_{\mathrm{ref,e}}$ is the cumulative refrigerating capacity of the traditional compression refrigeration system, kWh; COP_{ref} is the performance coefficient of the traditional compression refrigeration system.

(4) Levelized Annual Cost

The total levelized cost $C_{tot,L}$ is expressed as the sum of the initial levelized investment cost CI_L and the levelized fuel cost FC_L [36]. Values of parameters used in economic analysis are shown in Table 1.

$$C_{tot,L} = CI_L + FC_L \tag{40}$$

$$CI_L = (\sum_k Z_k + C_{INSTL})CRF \tag{41}$$

$$CRF = \frac{i(1+i)^n}{(1+i)^n - 1} \tag{42}$$

$$FC_L = c_f V_f \tag{43}$$

where $\sum_k Z_k$ is the equipment investment cost, CNY; C_{INSTL} is the equipment installation cost, CNY; CRF is the capital recovery factor; n is the system lifetime, year; c_f is the unit price of natural gas, CNY·m^{-3}; V_f is the natural gas consumption, m^3.

Table 1. Parameters value of economic analysis.

Parameter	Unit	Value
Absorption chiller	CNY·kW^{-1}	2000
Compression air conditioner	CNY·kW^{-1}	1000
Controllers	CNY	3000
Auxiliary heater	CNY	2000
Storage tank	CNY·m^{-3}	1000
Solar collector	CNY·m^{-2}	400
Natural gas price	CNY·m^{-3}	3
Electricity price	CNY·kWh^{-1}	1
Interest rate	%	4.9
System lifetime	years	25

(5) CO_2 Emissions Cost

In recent years, the problem of climate warming has become more and more serious due to the massive emission of greenhouse gases [37,38]. As the main component of greenhouse gases, CO_2 emissions have attracted much attention [39]. The calculated expression of carbon emission is as follows [40]:

$$CDE_{\mathrm{E}} = E_{\mathrm{E}} \cdot EF_{\mathrm{E}} \tag{44}$$

$$CDE_{\mathrm{NG}} = E_{\mathrm{NG}} \cdot EF_{\mathrm{NG}} \tag{45}$$

where E_E and E_{NG} are electricity consumption and natural gas consumption, respectively, kWh; EF_E and EF_{NG} are carbon emission factors of electricity and natural gas, respectively, kg·MWh^{-1}; CDE_E and CDE_{NG} are the CO_2 emissions of a compression refrigeration system and a solar single/double-effect LiBr-H_2O ARS, respectively, kg.

$$FC_E = CDE_E \cdot c_{CO_2} \quad (46)$$

$$FC_{NG} = CDE_{NG} \cdot c_{CO_2} \quad (47)$$

where c_{CO_2} is the unit CO_2 emission cost, CNY·kg^{-1}; FC_E and FC_{NG} are the carbon emission costs of a compression refrigeration system and a solar single/double-effect LiBr-H_2O ARS, respectively, CNY.

(6) Comprehensive Performance [41]

A single evaluation index could only reflect the advantages and disadvantages of a refrigeration system in one aspect, such as economic or environmental. In order to highlight the advantages of a solar single/double-effect switching LiBr-H_2O ARS, this study adopted the linear weighting method to construct a comprehensive evaluation index of economic and environmental indicators:

$$\min F = \varphi_1 FC + \varphi_2 CDE \quad (48)$$

where φ_1 and φ_2 are weight factors, with values of 0.6 and 0.4, respectively, and FC and CDE represent operating cost and carbon emissions, respectively, CNY and kg.

4. Results and Discussion

4.1. System Operation Performance

The weather data from 8 June to 14 June in Qingdao were selected to simulate and analyze the system. Qingdao is located in the temperate monsoon climate zone. The meteorological parameters of the Qingdao area were obtained using Meteonorm software and output in TYM format. The solar irradiance intensity changed obviously during this period, which reflected the characteristics of summer weather and had a certain degree of representativeness. The variations in solar irradiance intensity and ambient temperature from 8 June to 14 June are shown in Figure 2. Meanwhile, we set the time step of the simulation to 10 min during the simulation.

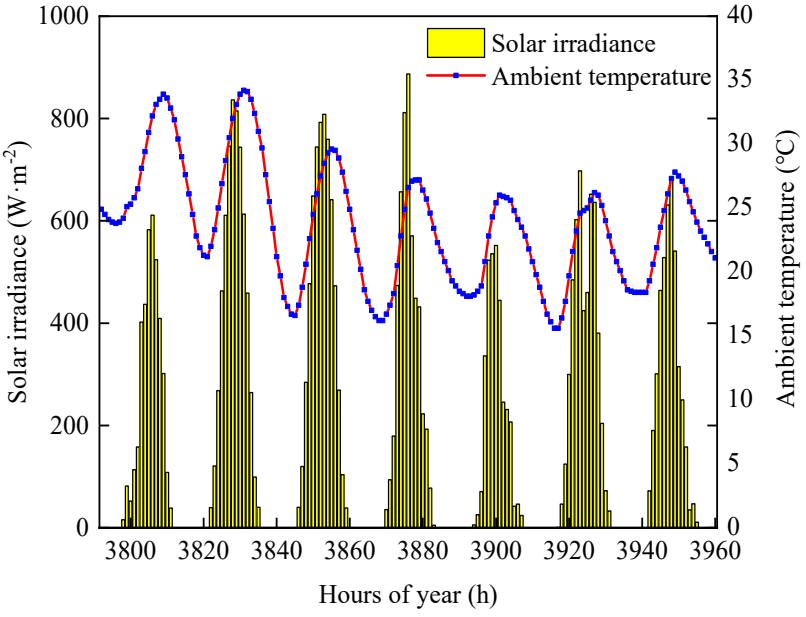

Figure 2. Data for solar irradiance and ambient temperature in Qingdao from June 8 to June 14.

4.1.1. Analysis of System Operation without Auxiliary Heater

In order to study the feasibility of a solar single/double-effect switching ARS, the daily cumulative cooling efficiency of the system was simulated without the auxiliary heater. The effect of the collector area and the storage tank volume on the daily cooling efficiency of the system is shown in Figure 3. On the first day of the simulation, the start-up time of the chiller was late, and the heat provided by the collector system was not enough to enable the refrigeration system to produce more cooling capacity, so the refrigeration efficiency was lower on that day. However, on the second day of the simulation, the daily cooling efficiency of the system increased rapidly. This was due to the high solar irradiance, and the water temperature in the storage tank was high on that day. Therefore, the system could operate in DEM at noon, and the *COP* of the system in DEM was higher. Compared with SEM, more refrigerant vapor could be generated by consuming less heat, and the heat source utilization rate was higher, which meant that the daily cooling efficiency was higher. However, with the decrease in the collector area, the temperature of the hot water in the water tank decreased, and the operating time of DEM also decreased, with the result that the daily cooling efficiency of the system decreased. On the third day of the simulation, the system could not operate in DEM when the collector area was reduced from 55 m^2 to 45 m^2, so the daily cooling efficiency dropped rapidly. However, Figure 2 shows that in the last three days of the simulation, the solar irradiation intensity in the Qingdao area was low, and the hot water was not enough to drive the system to operate in DEM even under the condition of 65 m^2 collector area. During these three days, the system only operated in SEM, so the daily cooling efficiency of the system changed little. Similarly, tank volume had the same effect on the daily cooling efficiency. Furthermore, it can be seen from the figure that the maximum daily cumulative cooling efficiency of the system was about 1, which showed that the system had good performance. Meanwhile, it can be seen from Figure 4 that under the initial conditions the system could switch between SEM and DEM without the auxiliary heater. However, the average daily cooling time of the system for one week was less than 10 h. Therefore, in order to study the operating characteristics of the system in practical application, it was necessary to install an auxiliary heater to prolong the cooling time of the system.

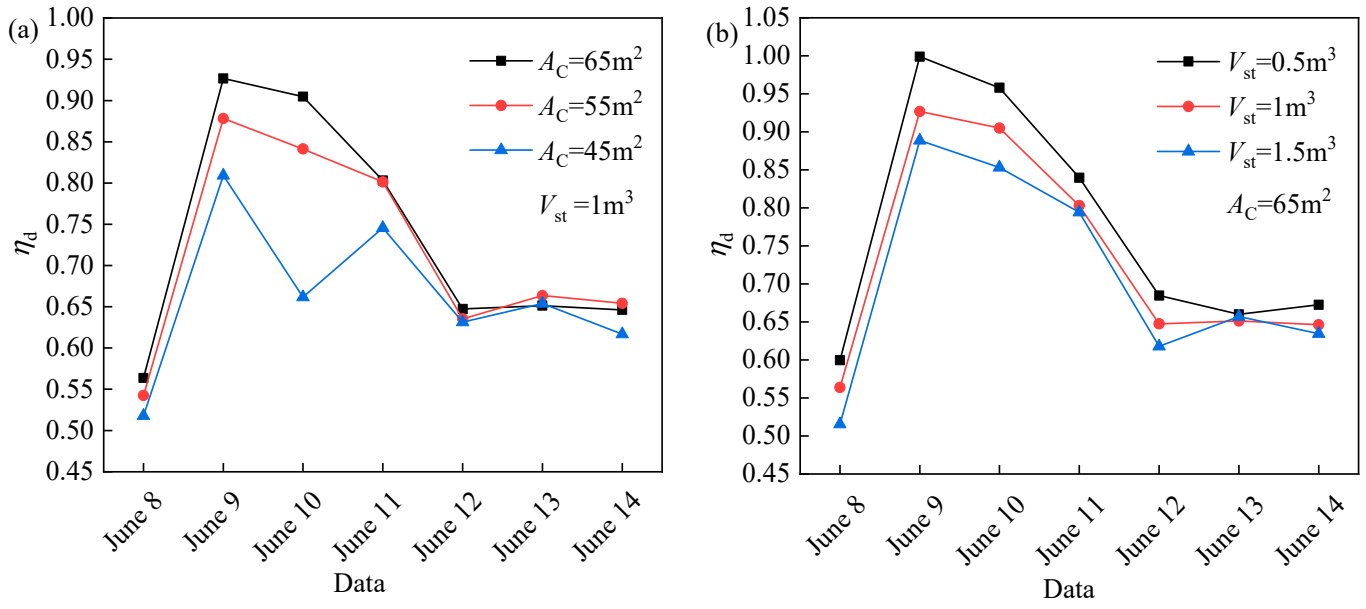

Figure 3. Variation in daily cooling efficiency with collector area and storage tank volume (**a**) collector area (**b**) storage tank volume.

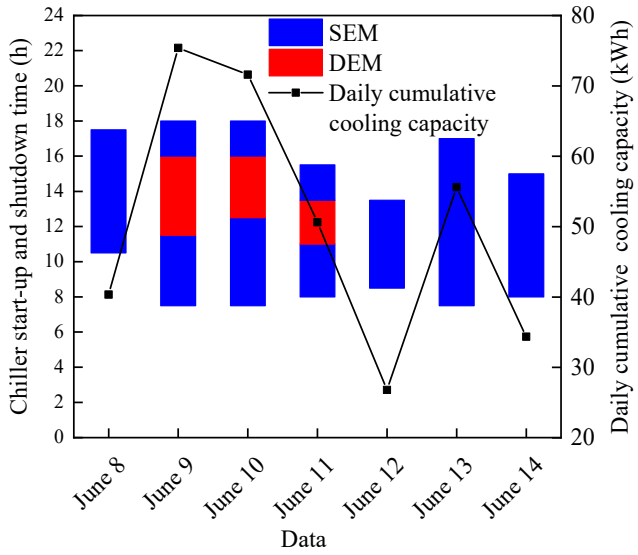

Figure 4. Daily single- and double-effect operation mode switching and daily cumulative cooling capacity of the system without auxiliary heater.

4.1.2. Analysis of System Operation with Auxiliary Heater

In order to study the actual operation characteristics of the solar single/double-effect LiBr-H_2O ARS and facilitate experimental verification in the future, a laboratory scale system with a daily cooling time of 7:00–19:00 was proposed. The design parameters of the system are shown in Table 2 and the operating parameters are shown in Table 3.

Table 2. Values for design parameters of the system.

Parameter	Unit	Value
Single-effect rated cooling capacity	kW	5
Double-effect rated cooling capacity	kW	10
Tank volume	m^3	1
Collector area	m^2	65
Collector slope	°	45
Longitude of Qingdao	°E	120.5
Latitude of Qingdao	°N	35.8

Table 3. Values for operating parameters of the system.

Parameter	Unit	Value
$\dot{m}_{p1}$	$kg{\cdot}s^{-1}$	0.83
$\dot{m}_{shwi}$	$kg{\cdot}s^{-1}$	0.3
T_{sawi}	°C	32
$\dot{m}_{sawi}$	$kg{\cdot}s^{-1}$	0.4
T_{scho}	°C	7
$\dot{m}_{scho}$	$kg{\cdot}s^{-1}$	0.3
$\dot{m}_{dhwi}$	$kg{\cdot}s^{-1}$	0.5
T_{dawi}	°C	32
$\dot{m}_{dawi}$	$kg{\cdot}s^{-1}$	1
T_{dcho}	°C	7
$\dot{m}_{dcho}$	$kg{\cdot}s^{-1}$	0.5

In the simulation of the operation characteristics of the system in practical application after continuous operation for one week, SEM was represented as Mode-1, DEM was represented as Mode-2 and the DEM driven by the auxiliary heater was represented as Mode-3. The daily operation mode switching of the system and the daily cumulative

cooling capacity of the system are shown in Figure 5. Due to the low solar irradiance intensity each morning, the heat storage temperature of the storage tank was low, which was not high enough to heat the hot water to the starting temperature of the chiller. Therefore, it was necessary to power on the auxiliary heater to heat the hot water to the DEM operating temperature, so that the system could operate in DEM. The temperature of the hot water in the storage tank did reach the start-up temperature of SEM with the increase in solar irradiance. Then, the auxiliary heat source was powered off, the hot water flowed to the SACH and the system operated in SEM. The solar irradiance intensity was high on the second, third and fourth days, and the heat storage temperature of the storage tank was able to reach the start-up temperature of DEM at noon. Therefore, hot water flowed to the DACH, and the system switched from SEM to DEM. The storage tank needed to continuously provide heat to the absorption chiller while storing heat; therefore, as the solar irradiation intensity decreased, the temperature of the storage tank also decreased, and the system switched to SEM or DEM driven by the auxiliary heater in the afternoons.

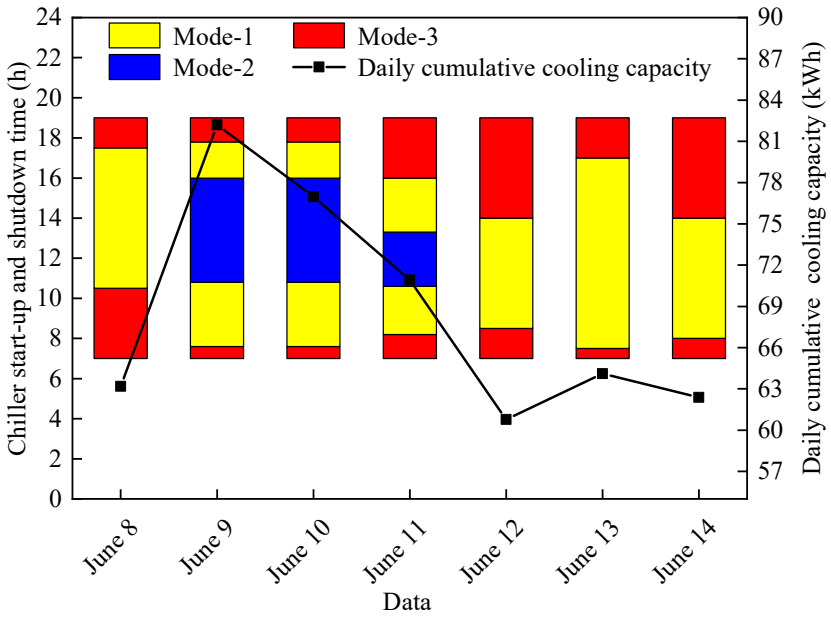

Figure 5. Daily single- and double-effect operation mode switching and daily cumulative cooling capacity of the system with auxiliary heater.

The hot water temperature and cooling capacity of the system for one week are shown in Figure 6. The outlet temperature of the water storage tank, the inlet temperature of the chilled water, the outlet temperature of the cooling water and the cooling capacity changed hourly. The highest outlet temperature of the hot water in the storage tank could reach 150 °C. The maximum cooling capacity of the system could be about 11 kW in DEM. The inlet temperature of chilled water varied in the range of 9.4–12.6 °C. The analysis results showed that the solar single/double-effect switching LiBr-H_2O ARS improved the utilization range of the heat source temperature (80–150 °C) of the solar refrigeration system. This indicated that the system was effective.

Meanwhile, taking the second day of the simulation as an example, the *COP* change of the chiller was analyzed. In the early morning and evening when the solar radiation intensity was low, the system operated in DEM driven by the auxiliary heater, and the *COP* of the chiller in this operation mode was about 1.26, which remained unchanged, as shown in Figure 7. At noon, the *COP* of the chiller in DEM could reach 1.33 at the highest with the increase in storage tank temperature. In addition, the *COP* in SEM varied from 0.67 to 0.72, and the average *COP* of the system on the second day was about 1.06, which was about 32.08−36.79% higher than that in SEM. The accumulative cooling capacity, auxiliary heat source consumption and heat stored in the storage tank in a week of system

operation are shown in Figure 8. The solar energy and auxiliary heat sources consumed by the system were 402.67 kWh and 105.84 kWh, respectively. Accumulative cooling capacity of 480.57 kWh was produced. The average *COP* of the system could be as high as 0.945. Because of the auxiliary heat source, the coefficient of performance was able to reach 4.54. The equivalent electric compression refrigeration performance coefficient was 10.09 (thermoelectric efficiency was 0.45).

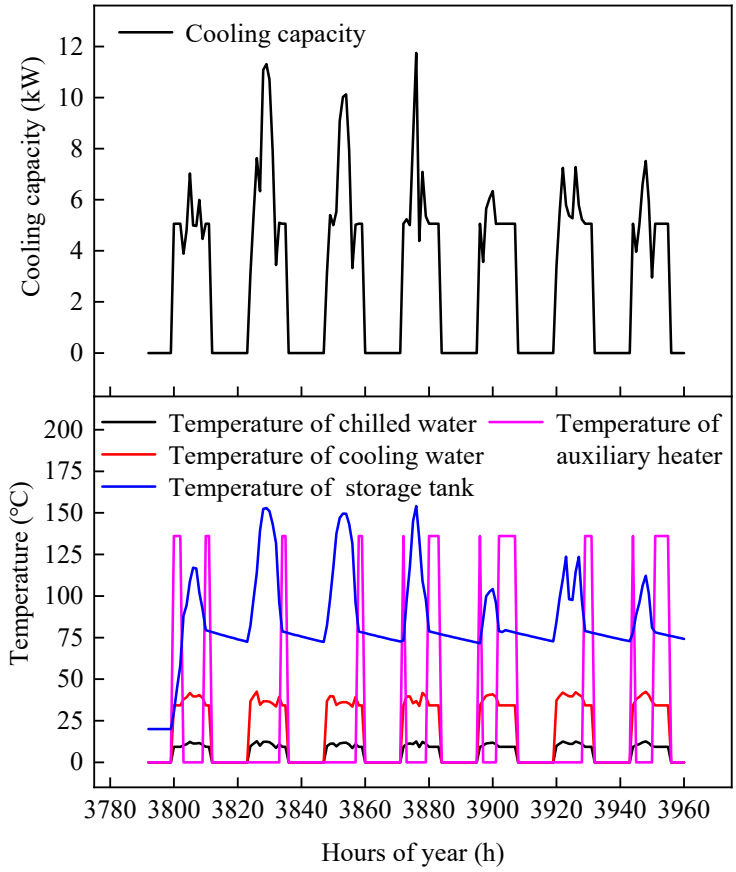

Figure 6. Dynamic condition of continuous operation of the system for one week.

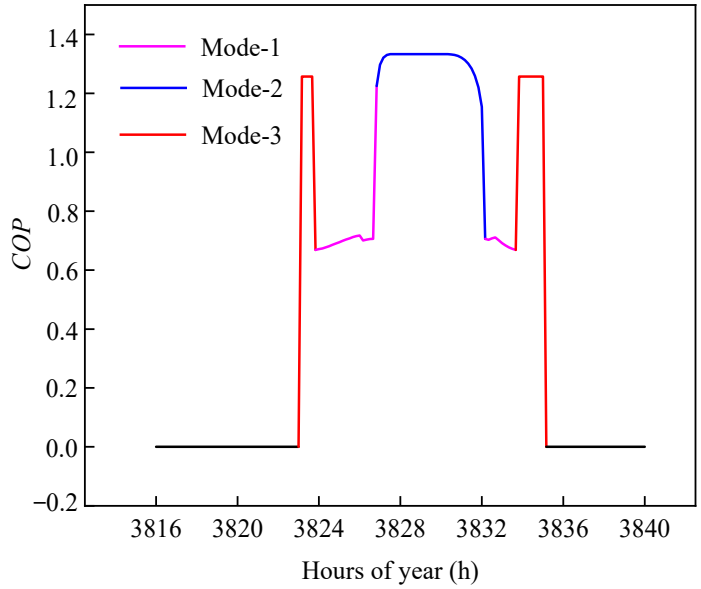

Figure 7. Variation of *COP* of chiller on the second day of simulation.

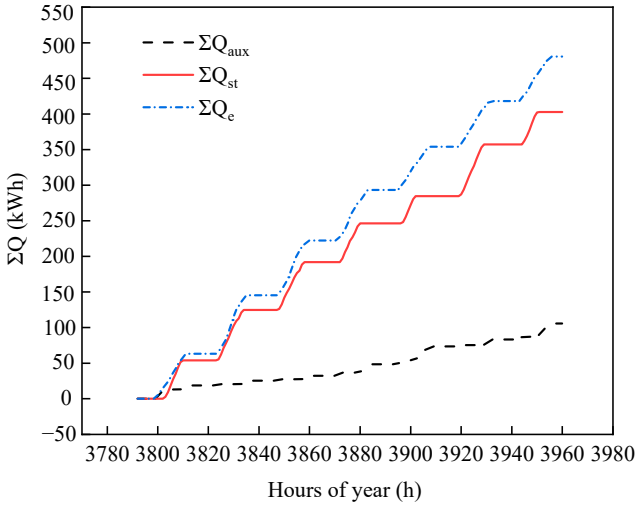

Figure 8. Accumulative cooling capacity, auxiliary heat source consumption, and heat stored in storage tank in a week of system operation.

Under the design condition of the system operating continuously for one week, the solar fraction of the system was 79.03%. For solar refrigeration systems, continuously improving the solar fraction and reducing the cost in order to improve their practicability and popularization is always an important research direction. However, the solar fraction is not only affected by uncontrollable factors such as weather conditions, but also by design and operation parameters such as the area of the collector, the volume of the storage tank, the temperature and flow rate of the external fluid, etc. The variation in solar energy fraction and primary energy saving rate with the collector area and the storage tank volume are shown in Figure 9. Obviously, increasing the area of the collector would increase the heat conversion of the collector and thus provide more heat to the chiller, which would help to reduce the use of auxiliary energy and increase the utilization fraction of solar energy. However, with the increase in collector area the cost would also increase, which was not conducive to the economy of the system. Compared with the compression refrigeration system, the primary energy saving rate of the system was about 0.34 under the setting conditions of 65 m^2 of collector area and 1 m^3 of storage tank volume. With the increase in collector area and storage tank volume, the heat-collecting capacity of the collectors and the heat-storage capacity of the storage tank increased, the solar fraction of the system increased, and the proportion of auxiliary energy utilization decreased; therefore, the primary energy saving rate of the system also increased.

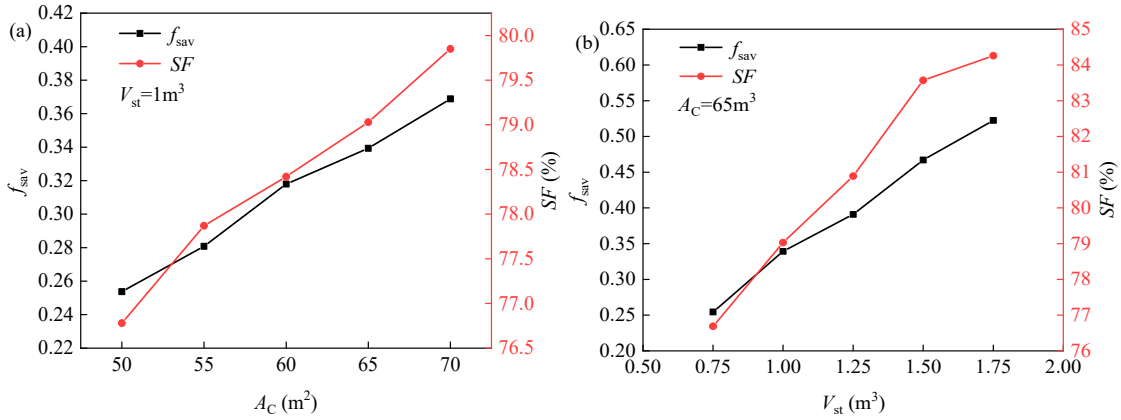

Figure 9. Variation of system *SF* and f_{sav} with collector area and storage tank volume (**a**) collector area (**b**) storage tank volume.

4.1.3. Analysis of System Operation in the Whole Refrigeration Season

In order to further highlight the advantages of the solar single/double-effect switching LiBr-H_2O ARS(C-1), the system was simulated for the whole refrigeration season (June to September). The solar fraction and auxiliary heat source consumption of the system were compared with the solar double-effect LiBr-H_2O ARS with auxiliary heat source(C-2). The comparison result is shown in Figure 10. It can be seen that the solar fraction of the solar single/double-effect switching LiBr-H_2O ARS operating continuously for the whole refrigeration season was about 71.99%, which was much higher than that of the solar double-effect LiBr-H_2O ARS. In contrast, the solar single/double-effect switching LiBr-H_2O ARS could save 1214.64 kWh of primary energy consumption by operating continuously for the whole refrigeration season.

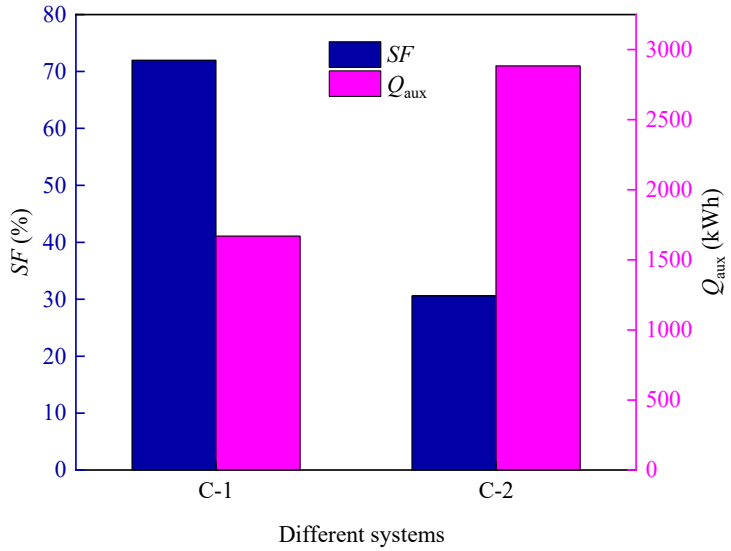

Figure 10. Comparison of solar fraction and auxiliary energy consumption of different systems operating continuously for the whole refrigeration season.

4.2. Economic Analysis

Economic analysis of solar refrigeration systems is helpful for improving the practicability and popularization of such systems, and it can also provide direction for their subsequent optimization. Therefore, in order to accurately evaluate the economic performance of the solar single/double-effect ARS, an annual economic analysis of the system was carried out by using the leveling cost. The system was operated continuously for the whole refrigeration season and then compared with the traditional compression refrigeration system. The comparison results are shown in Figure 11. It can be seen that the cost of the solar refrigeration system was divided into six parts, namely collector cost, absorption chiller cost, auxiliary heater cost, storage tank cost, controller cost and operation cost. Under the design conditions, the cost of the solar collector accounted for 37.60% of the total cost, and the cost of the single/double-effect absorption chiller accounted for 43.28% of the total cost. The initial investment cost of equipment accounted for 89.66%, while the operation cost only accounted for 10.34%. For the traditional compression refrigeration system with the same rated refrigeration capacity, the initial investment cost of equipment accounted for 17.45%, while the cost for a week of operation was CNY 1656, accounting for 82.55%, which was much higher than the solar single/double-effect switch LiBr-H_2O ARS. The price of the collector and the cost of the absorption chiller were still at a relatively high level—an important reason for the high initial investment cost of the solar refrigeration system. Improving the practicability and popularization of solar refrigeration systems could be achieved by reducing the cost of the collector and the absorption chiller. Therefore, it was of great significance that it had been possible to improve the utilization rate of solar energy, thereby reducing the cost of the solar refrigeration system. Moreover, the solar

single/double-effect switching ARS had the advantage of having a very low operating cost, something which could be further studied and used for popularization of the system in the future.

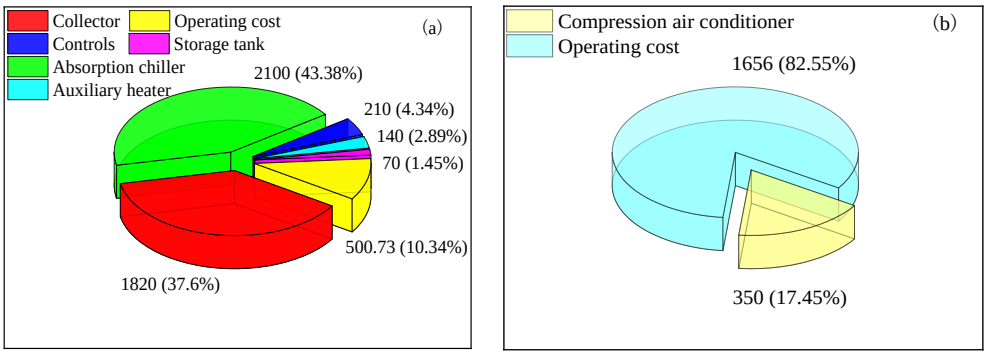

Figure 11. Levelized cost of solar refrigeration system and compression refrigeration system (**a**) solar refrigeration system (**b**) compression refrigeration system.

4.3. Environmental Analysis

The CO_2 emission, emission cost and comprehensive performance of the solar single/double-effect ARS for the whole refrigeration season were analyzed and compared with other forms of refrigeration systems. The CO_2 emission of the solar single/double-effect refrigeration system was compared with that of a solar double-effect LiBr-H_2O ARS (C-2) and a compression refrigeration system (C-3), as shown in Figure 12. The CO_2 emissions of the three refrigeration systems were 307.11 kg, 1034.27 kg and 1251.9 kg, respectively. Compared with the traditional compression refrigeration system and the solar double-effect ARS, the CO_2 emission of the solar single/double-effect refrigeration system was reduced by 75.47% and 70.31%, respectively. Meanwhile, the CO_2 emission costs of the three refrigeration systems were CNY 15.36, CNY 51.71 and CNY 62.60, respectively. Therefore, the solar single/double-effect refrigeration system had better environmental benefits.

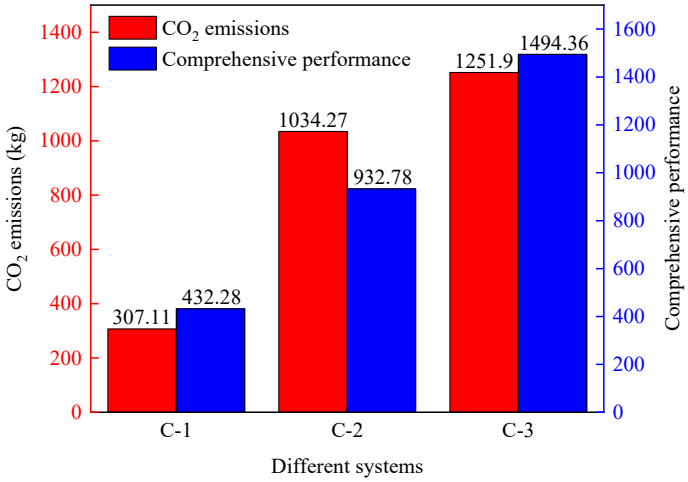

Figure 12. Comparison of CO_2 emissions and comprehensive performance of different systems.

In order to adequately reflect the advantages of the system, the comprehensive performance of the solar single/double switching refrigeration system was compared with other forms of solar refrigeration systems. The comprehensive performance evaluation index synthesized the operating cost and environmental benefit of the system and put the economic benefit in the first place, giving it a higher weight. The comprehensive evaluation index values for the solar single/double-effect switching LiBr-H_2O ARS, the solar double-effect LiBr-H_2O ARS and the traditional compression refrigeration system were 432.28, 932.78 and 1494.36, respectively. Therefore, the comprehensive performance

of the solar single/double-effect switching LiBr-H_2O ARS was better than the other two systems. Therefore, the solar single/double-effect switching ARS had great advantages. In the future, with the reduction in the cost of collectors and heat exchangers, the system is expected to be widely popularized and applied.

5. Conclusions

In order to improve the utilization range of the heat source temperature in solar refrigeration systems and make full use of solar energy, the modeling and simulation of the solar single/double-effect LiBr-H_2O ARS were performed in this study. In addition, in order to study the feasibility of the solar single/double-effect LiBr-H_2O ARS, an economic analysis and an environmental analysis of the system were carried out. The main conclusions drawn from this study can be summarized as follows:

(1) In weather conditions of high solar irradiation, the system could be switched between single- and double-effect modes. Due to the high *COP* of the DACH, the daily cooling efficiency of the system was high in weather conditions that triggered double-effect operation, and there was an obvious change in this measure when changes were made to the collector area and the storage tank volume.

(2) Under the design conditions, the solar fraction of the system was 79.03%, much higher than that of the solar double-effect LiBr-H_2O ARS with auxiliary heater, and increased with the increase in the storage tank volume and the collector area. Compared with the compression refrigeration system, the solar single/double-effect switching LiBr-H_2O ARS could achieve a primary energy saving rate of 25–52% in a certain range. Compared with the solar double-effect LiBr-H_2O ARS, the solar single/double-effect switching LiBr-H_2O ARS could save 1214.64 kWh of primary energy consumption during continuous operation for the whole refrigeration season.

(3) A high initial investment cost and a low operation cost are typical characteristics of solar ARSs. Compared with the traditional compression refrigeration system, the initial investment cost of the solar single/double-effect LiBr-H_2O ARS was higher, accounting for 89.66% of the total levelized cost, but its operating cost was lower. Meanwhile, the CO_2 emission of the solar single/double-effect switching refrigeration system was 75.47% and 70.31% lower than that of the traditional compression refrigeration system and the solar double-effect ARS, respectively. The emission reduction effect of the solar single/double-effect switching ARS was obvious.

Author Contributions: Q.L.: Conceptualization, Methodology, Investigation, Writing—original draft. S.Z. (Shiqi Zhao): Methodology, Software, Writing—review and editing. D.W.: Conceptualization, Methodology, Writing—review and editing, Project administration, Funding acquisition. Q.S.: Writing—review and editing, Supervision. S.Z. (Sai Zhou): Methodology, Software, Writing—review and editing. X.W.: Methodology, Writing—review and editing. Y.L.: Methodology, Writing—review and editing, Project administration. All authors have read and agreed to the published version of the manuscript.

Funding: This work was funded by the National Natural Science Foundation of China under contract No. 51876094.

Data Availability Statement: The data used to support the findings of this study are available from the corresponding author upon request.

Conflicts of Interest: The authors declare no conflict of interest.

Nomenclature

A	area (m^2)
c	unit cost of natural gas (CNY·m^{-3})
CDE	CO_2 emissions (kg)
CI	capital investment cost (CNY)
$CINST$	installation cost (CNY)

COP	coefficient of performance (–)
cp	specific heat at constant pressure (kJ·kg^{-1}·°C^{-1})
CRF	capital recovery factor (–)
$C_{tot,L}$	total cost (CNY)
FC	fuel cost (CNY)
f_{sav}	primary energy saving rate (–)
h	enthalpy (kJ·kg^{-1})
i	interest rate (%)
K	heat transfer coefficient (W·m^{-2}·°C^{-1})
m	mass flow rate (kg·s^{-1})
n	system lifetime (year)
η	heat exchange efficiency
q_r	latent heat of vaporization (kJ·kg^{-1})
Q	heat transfer rate (kW)
Qe	cooling capacity (kW)
SF	solar fraction
T	temperature (°C)
V	volume (m^3)
x	solution mass fraction
Z	purchased equipment cost (CNY)
Subscripts	
ARS	absorption refrigeration system
AB,ab	absorber
aux	auxiliary
awi	cooling water inlet
c	collector
cho	chilled water outlet
CHW	chilled water
CON	condenser
CW	cooling water
DACH	double-effect absorption chiller
DEM	double-effect mode
d	double-effect
EVA,e	evaporator
E	electric
EV	electric valve
f	fuel
GEN,g	generator
HG,hg	high pressure generator
HW	hot water
hwi	hot water inlet
i	set-point
in	input
L	levelized
LG,lg	low pressure generator
NG	natural gas
out	output
p	pump
s	single-effect
SACH	single-effect absorption chiller
SEM	single-effect mode
SC	solar collector
ST,st	storage tank
v	vapor

References

1. Rodriguez-Toscano, A.; Amaris, C.; Sagastume-Gutierrez, A.; Bourouis, M. Technical, environmental, and economic evaluation of a solar/gas driven absorption chiller for shopping malls in the Caribbean region of Colombia. *Case Stud. Therm. Eng.* **2022**, *30*, 101743. [CrossRef]
2. Alobaid, M.; Hughes, B.; Calautit, J.K.; O'Connor, D.; Heyes, A. A review of solar driven absorption cooling with photovoltaic thermal systems. *Renew. Sustain. Energy Rev.* **2017**, *76*, 728–742. [CrossRef]
3. Mortadi, M.; El Fadar, A. Performance, economic and environmental assessment of solar cooling systems under various climates. *Energ. Convers. Manag.* **2022**, *252*, 114993. [CrossRef]
4. Ayou, D.S.; Coronas, A. New Developments and Progress in Absorption Chillers for Solar Cooling Applications. *Appl. Sci.* **2020**, *10*, 4073. [CrossRef]
5. Aliane, A.; Abboudi, S.; Seladji, C.; Guendouz, B. An illustrated review on solar absorption cooling experimental studies. *Renew. Sustain. Energy Rev.* **2016**, *65*, 443–458. [CrossRef]
6. Barbosa, J.M.; Andrade, L.A.; Vieira, L.G.M.; Barrozo, M.A.S. Multi-response optimization of bio-oil production from catalytic solar pyrolysis of Spirulina platensis. *J. Energy Inst.* **2020**, *93*, 1313–1323. [CrossRef]
7. Bataineh, K.M.; Alrifai, S. Recent trends in solar thermal sorption cooling system technology. *Adv. Mech. Eng.* **2015**, *7*, 1687814015586120. [CrossRef]
8. Cerezo, J.; Lara, F.; Romero, R.J.; Rodriguez, A. Analysis and Simulation of an Absorption Cooling System Using a Latent Heat Storage Tank and a Tempering Valve. *Energies* **2021**, *14*, 1376. [CrossRef]
9. Xu, Z.Y.; Wang, R.Z. Simulation of solar cooling system based on variable effect LiBr-water absorption chiller. *Renew. Energy* **2017**, *113*, 907–914. [CrossRef]
10. Figaj, R.; Zoladek, M. Experimental and numerical analysis of hybrid solar heating and cooling system for a residential user. *Renew. Energy* **2021**, *172*, 955–967. [CrossRef]
11. Chen, L.; Jin, S.M.; Bu, G.F. Experimental investigation of a novel multi-tank thermal energy storage system for solar-powered air conditioning. *Appl. Therm. Eng.* **2017**, *123*, 953–962. [CrossRef]
12. Singh, G.; Das, R. Experimental Study on a New Small-Scale Absorption System: Response Surface and Inverse Analyses. *J. Energ. Resour. Technol.* **2021**, *143*, 092103. [CrossRef]
13. Shirazi, A.; Taylor, R.A.; Morrison, G.L.; White, S.D. Solar-powered absorption chillers: A comprehensive and critical review. *Energ. Convers. Manag.* **2018**, *171*, 59–81. [CrossRef]
14. Sun, S.; Zhang, K.; Song, Q.; Wang, D.; Li, Y.; Kong, X. Experimental research on heat and mass transfer characteristics of membrane energy accumulator used in solar refrigeration. *Int. J. Refrig.* **2021**, *128*, 186–196. [CrossRef]
15. Sun, S.; Sun, H.; Song, Q.; Wang, D.; Kong, X.; Li, Y. Comparative analysis of energy discharge characteristics between hollow fiber membrane and flat membrane energy accumulators. *Int. J. Refrig.* **2021**, *131*, 874–886. [CrossRef]
16. Iranmanesh, A.; Mehrabian, M.A. Dynamic simulation of a single-effect LiBr–H_2O absorption refrigeration cycle considering the effects of thermal masses. *Energ. Build.* **2013**, *60*, 47–59. [CrossRef]
17. Cheng, Y.L.; Liu, M.; Liu, Z.D.; Zhan, C.L. Operation analysis and optimization study of a small absorption refrigeration system driven by flat plate collector. *Renew. Energy Resour.* **2021**, *41*, 1023–1029.
18. Shirazi, A.; Taylor, R.A.; White, S.D.; Morrison, G.L. A systematic parametric study and feasibility assessment of solar-assisted single-effect, double-effect, and triple-effect absorption chillers for heating and cooling applications. *Energ. Convers. Manag.* **2016**, *114*, 258–277. [CrossRef]
19. Siddique, M.Z.; Badar, A.W.; Siddiqui, M.S.; Butt, F.S.; Saleem, M.; Mahmood, K.; Fazal, I. Performance analysis of double effect solar absorption cooling system with different schemes of hot/cold auxiliary integration and parallel-serial arrangement of solar field. *Energy* **2022**, *245*, 123299. [CrossRef]
20. Hang, Y.; Qu, M.; Winston, R.; Jiang, L.; Widyolar, B.; Poiry, H. Experimental based energy performance analysis and life cycle assessment for solar absorption cooling system at University of Californian, Merced. *Energ. Build.* **2014**, *82*, 746–757. [CrossRef]
21. Rahman, S.; Said, Z.; Issa, S. Performance evaluation and life cycle analysis of new solar thermal absorption air conditioning system. *Energy Rep.* **2020**, *6*, 673–679. [CrossRef]
22. Narayanan, R.; Harilal, G.K.; Golder, S. Feasibility study on the solar absorption cooling system for a residential complex in the Australian subtropical region. *Case Stud. Eng.* **2021**, *27*, 101202. [CrossRef]
23. Figaj, R.; Szubel, M.; Przenzak, E.; Filipowicz, M. Feasibility of a small-scale hybrid dish/flat-plate solar collector system as a heat source for an absorption cooling unit. *Appl. Therm. Eng.* **2019**, *163*, 114399. [CrossRef]
24. Xu, Z.Y.; Wang, R.Z. Comparison of CPC driven solar absorption cooling systems with single, double and variable effect absorption chillers. *Sol. Energy* **2017**, *158*, 511–519. [CrossRef]
25. Zhang, K.; Ma, H.; Li, Q.; Wang, D.; Song, Q.; Wang, X.; Kong, X. Thermodynamic analysis and optimization of variable effect absorption refrigeration system using multi-island genetic algorithm. *Energy Rep.* **2022**, *8*, 5443–5454. [CrossRef]
26. Ke, Z.; Haijing, M.; Honglei, S.; Dechang, W.; Xiaohe, W.; Qinglu, S. Parameter Evaluation of Variable Effect Lithium Bromide Absorption Refrigeration Cycles Based on ANOVA. *J. Refrig.* **2022**, *43*, 137–144. [CrossRef]
27. Lubis, A.; Jeong, J.; Giannetti, N.; Yamaguchi, S.; Saito, K.; Yabase, H.; Alhamid, M.I.; Nasruddin. Operation performance enhancement of single-double-effect absorption chiller. *Appl. Energy* **2018**, *219*, 299–311. [CrossRef]

28. Alhamid, M.I.; Coronas, A.; Lubis, A.; Ayou, D.S.; Nasruddin; Saito, K.; Yabase, H. Operation strategy of a solar-gas fired single/double effect absorption chiller for space cooling in Indonesia. *Appl. Therm. Eng.* **2020**, *178*, 115524. [CrossRef]
29. Ma, H.; Li, Q.; Wang, D.; Song, Q.; Zhou, S.; Wang, X.; Li, Y. Operating performance and economic analysis of solar single/double-effect compound absorption refrigeration system. *Sol. Energy* **2022**, *247*, 73–85. [CrossRef]
30. Qing, C. *Analysis of Operating Characteristics of Solar Lithium Bromide Absorption Unit*; North China Electric Power University: Qingdao, China, 2020. [CrossRef]
31. Ibrahim, N.I.; Al-Sulaiman, F.A.; Ani, F.N. A detailed parametric study of a solar driven double-effect absorption chiller under various solar radiation data. *J. Clean Prod.* **2020**, *251*, 119750. [CrossRef]
32. Rejeb, O.; Ghenai, C.; Bettayeb, M. Modeling and simulation analysis of solar absorption chiller driven by nanofluid-based parabolic trough collectors (PTC) under hot climatic conditions. *Case Stud. Eng.* **2020**, *19*, 100624. [CrossRef]
33. Wageiallah Mohammed, O.; Yanling, G. Comprehensive Parametric Study of a Solar Absorption Refrigeration System to Lower Its Cut In/Off Temperature. *Energies* **2017**, *10*, 1746. [CrossRef]
34. Bagheri, B.S.; Shirmohammadi, R.; Mahmoudi, S.M.S.; Rosen, M.A. Optimization and comprehensive exergy-based analyses of a parallel flow double-effect water-lithium bromide absorption refrigeration system. *Appl. Therm. Eng.* **2019**, *152*, 643–653. [CrossRef]
35. Abrudan, A.C.; Pop, O.G.; Serban, A.; Balan, M.C. New Perspective on Performances and Limits of Solar Fresh Air Cooling in Different Climatic Conditions. *Energies* **2019**, *12*, 2113. [CrossRef]
36. Mehmood, S.; Maximov, S.A.; Chalmers, H.; Friedrich, D. Energetic, Economic and Environmental (3E) Assessment and Design of Solar-Powered HVAC Systems in Pakistan. *Energies* **2020**, *13*, 4333. [CrossRef]
37. Esfandi, S.; Baloochzadeh, S.; Asayesh, M.; Ehyaei, M.A.; Ahmadi, A.; Rabanian, A.A.; Das, B.; Costa, V.A.F.; Davarpanah, A. Energy, Exergy, Economic, and Exergoenvironmental Analyses of a Novel Hybrid System to Produce Electricity, Cooling, and Syngas. *Energies* **2020**, *13*, 6453. [CrossRef]
38. Sadi, M.; Arabkoohsar, A. Exergy, economic and environmental analysis of a solar-assisted cold supply machine for district energy systems. *Energy* **2020**, *206*, 118210. [CrossRef]
39. Liu, L.; Li, Z.; Jing, Y.; Lv, S. Energetic, economic and environmental study of cooling capacity for absorption subsystem in solar absorption-subcooled compression hybrid cooling system based on data of entire working period. *Energ. Convers. Manag.* **2018**, *167*, 165–175. [CrossRef]
40. Shirazi, A.; Taylor, R.A.; White, S.D.; Morrison, G.L. Transient simulation and parametric study of solar-assisted heating and cooling absorption systems: An energetic, economic and environmental (3E) assessment. *Renew. Energy* **2016**, *86*, 955–971. [CrossRef]
41. Li, J.; Yao, Y.; Liu, B. Optimization operation of comprehensive energy system based on comprehensive evaluation index. *J. Guangxi Univ. Nat. Sci. Ed.* **2022**, *47*, 1518–1531. [CrossRef]